Peer reviewed version

University of Bristol - Explore Bristol Research
General rights

Ice fabric in an Antarctic ice stream interpreted from seismic anisotropy

Emma C. SMITH[1,2]*, **Alan F. BAIRD**[3], **J. Michael KENDALL**[3], **Carlos MARTÍN**[1], **Robert S. WHITE**[2], **Alex M. BRISBOURNE**[1], **Andrew M. SMITH**[1]

[1]British Antarctic Survey, Natural Environment Research Council,Cambridge, CB3 0ET, UK
[2]Bullard Laboratories, Department of Earth Sciences, University of Cambridge, Cambridge, CB3 0EZ, UK
[3]School of Earth Sciences, University of Bristol, Wills Memorial Building, Bristol, BS8 1RJ, UK

Key Points:

- Anisotropic ice fabric in an Antarctic ice stream measured using seismic shear wave splitting
- Measured fabric results in ice shearing 9.1 times more easily along flow direction than across flow
- The measured fabric has strong implications for parametrising data-driven models of past and future ice flow

*Current address: Alfred-Wegener-Institut für Polar- und Meeresforschung, Bremerhaven, Germany

Corresponding author: Emma C. Smith, `emma.smith@awi.de`

Abstract

Here we present new measurements of an anisotropic ice fabric in a fast moving (377 ma^{-1}) ice stream in West Antarctica. We use ~6000 measurements of shear wave splitting observed in microseismic signals from the bed of Rutford Ice Stream, to show that in contrast to large-scale ice flow models, which assume that ice is isotropic, the ice in Rutford Ice Stream is dominated by a previously unobserved type of partial girdle fabric. This fabric has a strong directional contrast in mechanical properties, shearing 9.1 times more easily along the ice flow direction than across flow. This observed fabric is likely to be widespread and representative of fabrics in other ice streams and large glaciers, suggesting it is essential to consider anisotropy in data-driven models to correctly predict ice loss and future flow in these regions. We show how passive microseismic monitoring can be effectively used to provide these data.

1 Introduction

As ice flows, its internal structure changes in response to the stresses it has encountered. Understanding the types of structure, known as ice fabrics, formed in different flow environments is needed for accurate prediction of the future behaviour of ice sheets using ice flow models [*Azuma*, 1994]. Glacial ice is formed of hexagonal ice crystals, known as Ih ice [*Faria et al.*, 2014a]. These crystals are strongly anisotropic, the viscosity is around 60 times less along the basal plane (normal to the c-axis) than perpendicular to it [*Duval et al.*, 1983], meaning the ice is softer and deforms preferentially on this plane by slip (ice creep). This causes c-axes in a bulk polycrystalline ice mass to rotate when under stress, forming a preferred crystal orientation fabric (COF) which is also anisotropic. The type of COF formed records the deformation history of ice and the viscosity of the COF will affect future ice flow [*Alley*, 1988]. *In situ* measurements of ice COF are most commonly made over slow moving ice at ridges and domes (e.g. *Faria et al.* [2014a,b]; *Matsuoka et al.* [2012]) with very few measurements made in fast moving ice stream environments. Ice streams are the key discharge pathways of the Greenland and Antarctic ice sheets. Lack of observational data in these key regions limits our ability to model their flow and evolution [*Gagliardini et al.*, 2009] and thus the future of the ice sheets themselves and their contribution to global sea level. Here we present measurements of a strong ice fabric in Rutford Ice Stream, Antarctica. We measure seismic shear wave anisotropy observed in icequake signals generated at the base of Rutford Ice Stream to assess the ice fabric properties in this region.

2 Site Location and Observed Shear Wave Splitting

In Rutford Ice Stream, Antarctica, 40 km upstream of the grounding line, the ice flows at an average velocity of 377 ma^{-1} [*Murray et al.*, 2007]. In this area the ice is around 2.2 km thick and 25 km wide (Fig. 1a) and has been flowing in a laterally-confined ice stream environment for around 150 km. As the ice flows, seismicity is generated by basal sliding over 'sticky spots' at the base of the ice stream [*Smith*, 2006; *Smith et al.*, 2015]. Seismic energy radiates outwards from the source as elastic body waves, longitudinal P-waves and transverse S-waves (shear waves), which are detected by three-component receivers at the ice surface (Fig. 1b). A clear indication that these elastic waves have travelled through an anisotropic ice fabric is the presence of two independent S-waves (S1 and S2, Fig. 1b). When an S-wave, generated at the base of the ice stream, encounters a region of anisotropic ice it will split into two orthogonal S-waves, this is known as shear wave splitting (SWS) or seismic birefringence. The two split S-waves propagate independently, arriving at a receiver separated by a delay time and with directions of polarisation controlled by the anisotropic symmetry axis of the fabric they have traveled through [*Savage*, 1999]. We measure this delay time (δt), which is proportional to the strength of

anisotropy, and the polarisation direction of the fastest S-wave (Φ), which is an indicator of the anisotropic symmetry of the medium.

The data set used in this study contains ~3000 basal seismic events with high signal to noise ratio S-waves, recorded at 10 receivers [*Smith et al.*, 2015]. This means there are ~30,000 shear wave splitting measurements to be made, one for each pair of shear wave arrivals on each station for each event. We use the automated approach of *Wuestefeld et al.* [2010] to make these measurements, which provides an effective method of processing a large quantity of data. Ray paths from each event to each station cover a variety of azimuths and inclinations, which allows us to effectively sample the ice fabric in this area and derive the elastic anisotropy. From the elastic anisotropy we then infer the *in situ* anisotropic ice COF.

3 Shear Wave Splitting Analysis and Results

The automated method of *Wuestefeld et al.* [2010] determines the combination of polarisation direction of the fastest S-wave (Φ) and delay time (δt) which best remove the effects of shear-wave splitting for each of the ~30,000 pairs of shear waves in this dataset. The method also calculates an automated quality factor (Q) of the resulting shear wave splitting measurements which can then be used to filter the results by determining a threshold of Q above which the measurements are of a suitable quality. Before the data were processed the seismic waveforms for each event were rotated into geographical: East, North, Vertical (ENZ) orientation from the field orientation of XYZ. Waveforms were not rotated into the ray frame before analysis, as is commonly the case for SWS analysis. Arrivals in this data set are near vertical, due to refraction caused by a low velocity firn layer at the surface (~100 m in thickness). This means the majority of the S-wave energy is recorded on the horizontal components (E and N), which will be used in the SWS analysis, and therefore rotation is not necessary.

The method of *Wuestefeld et al.* [2010] can be summarised as follows: An analysis time window is defined around the picked S-wave arrivals on the horizontal (E and N) components of a station. Within this window a robust grid search is performed over all possible values of polarisation directions (-90° < Φ < 90°) and delay time (0 s < δt < 0.1 s). As the analysis is very sensitive to the length of the analysis time window [*Teanby et al.*, 2004], the analysis is repeated for a range of window lengths. The values of Φ and δt which are most stable over this range of window lengths is assessed using the cluster analysis method of *Teanby et al.* [2004]. The combination of parameters that provides the best removal of splitting is assessed using two different methods. The first, the XC method, is based on cross-correlating the corrected S-wave waveforms to assess similarity. The second, the EV method, is based on assessing the extent to which particle motion of the corrected waveforms has been linearised, using the method of *Silver and Chan* [1991]. A comparison between the values of the splitting parameters, Φ and δt, determined using the two methods allows the automated identification of good results by calculating a quality factor (Q), where Q = 1 indicates a good splitting measurement. By manual inspection of a sub-set of the results, splitting measurements with a signal-to-noise ratio > 7.5 and Q > 0.8 were selected yielding a total of 5951 shear wave splitting measurements.

The strength of the anisotropy along a ray path can be expressed as a percentage difference in velocity between the fast and slow waves using

$$\delta V_s = (\overline{V_s} \times \delta t \times 100)/r, \qquad (1)$$

where $\overline{V_s}$ = 1944 ms^{-1}, is the average isotropic S-wave velocity and r is the source-receiver straight line distance for a given measurement (details on event location given in *Smith et al.* [2015]). It should be noted, that while the arrivals are refracted in the near-surface firn layer, the majority of the travel-path of a given shear-wave is in the ice column. This means a source-receiver straight line distance is a reasonable approximation for the true

travel path (differences at maximum offset are around 10-20 m, which is within the location error - details in *Smith et al.* [2015]).

The resulting values plotted on an upper hemisphere projection (Fig. 2) show that SWS measurements cover a wide range of ray path azimuths, and inclinations out to 73°. The measurements show that the dominant polarisation direction of the fast S-wave (Φ) is perpendicular to the ice flow direction and the strongest seismic anisotropy (δV_s) occurs in the near vertical ray paths. There is no systematic variation in Φ for different regions of the ice stream suggesting the ice fabric in this area is uniform and all measurements can be treated as sampling the same fabric at a variety of ray azimuths and inclinations. The measurements show a clear trend of greatest δV_s in the vertical (centre of the plot), weakening with increasing inclination angle (edge of the plot). There are also azimuthal variations in δV_s and Φ, which are especially evident for ray paths with inclinations of 30° to 60°.

4 Modeling for Ice COF

In order to determined the type of ice fabric that would cause this pattern of shear-wave splitting we use a forward model of elastic wave propagation through anisotropic ice fabrics to calculate the theoretical SWS for a given ice fabric type. Elasticity tensors derived from *Maurel et al.* [2015] are used to determine the phase velocities, and thus the modelled shear wave splitting parameters ($\delta V_{s\,M}$ and Φ_M) associated with S-waves travelling through the specified fabric at different azimuths and inclinations.

To define the misfit between measured and modeled splitting parameters, we first express them as vectors (with lengths δV_s and $\delta V_{s\,M}$, and orientations Φ and Φ_M respectively). The two are then subtracted to find the residual vector. The global misfit, f, to be minimised in our inversion is simply the summation of the magnitude of the residuals for all n of the SWS measurements:

$$f = \sum_n \sqrt{(\delta V_s sin2\Phi - \delta V_{s\,M} sin2\Phi_M)^2 + (\delta V_s cos2\Phi - \delta V_{s\,M} cos2\Phi_M)^2}, \qquad (2)$$

the factor of 2 in the trigonometric functions in (2) accounts for the fact that Φ has 180° periodicity rather than 360°. It should be noted that prior to this process, measured SWS values are averaged within inclination and azimuth bins of 5°$\times$ 5° in order to avoid a systematic bias in the model fit to regions where there are a higher density of measurements.

Fabrics commonly observed elsewhere in ice, transversely isotropic with either vertical or horizontal axes of symmetry (VTI, HTI), can be eliminated as the sole cause of anisotropy in this survey area [*Harland et al.*, 2013] for the following reasons: pure VTI (cluster fabric) would show a minimum δV_s for vertically-propagating waves, and pure HTI (thick girdle) would show high δV_s across all inclinations perpendicular to the ice flow direction (Fig. 3), neither of which match the observations (Fig. 2). Therefore, three polycrystaline ice fabric models were tested, combining a cluster fabric with varying degrees of three different girdle fabrics (Fig. 3): a thick girdle, a vertical partial girdle (partial girdle of *Maurel et al.* [2015]) and a horizontal partial girdle fabric (vertical partial girdle rotated 90° in the X_2 plane). The elasticity tensors describing these mixed fabric models are calculated using a Voigt-Reuss-Hill average [*Hill*, 1952]. For each of the three starting models, the misfit (Equation 2) is calculated for all variable parameters (opening angles and proportions of each input fabric) to indicate the fabric model which best fits the data.

The ice fabric model that provides the best fit to the observed SWS measurements is comprised of a mixture of 47% horizontal partial girdle (HPG), an orthorhombic fabric with a narrow opening angle of $\theta = 22°$, orientated near orthogonal to the ice flow direction (Fig. 4a) and 53% cluster fabric with an opening angle of $\theta = 73°$ (Fig. 4b). While partial girdle fabrics have been commonly hypothesised in the literature (e.g. *Nanthikesan*

and Shyam Sunder* [1994]; *Maurel et al.* [2015]; *Diez and Eisen* [2015]) the HPG ice fabric has not been observed in glacial ice before; henceforth we refer to the mixed HPG and cluster fabric as 'diffuse HPG'.

5 Discussion

The fit between modeled SWS results using the diffuse HPG fabric model and the observed SWS measurements is very good (Fig. 4c) with an average misfit per measurement of only ~1.2%. Both the orientation of the fast S-wave and the pattern in strength of splitting match well. The azimuthal variation in the pattern of splitting is recreated well by the ice fabric model, for example the lobes of alternating high and low δV_s between 30° and 60° ray path inclination. There are relatively few measurements where lobes of high δV_s are modeled at 50° and 230° azimuth at high inclinations; these are the only areas where the model cannot be tested. In the diffuse HPG fabric the pattern of S-wave anisotropy is largely influenced by the HPG component, as can be seen by comparing Fig. 4a and Fig. 4c. The cluster component of diffuse HPG (Fig. 4b) is broad and as a fabric it has a low degree of anisotropy, verging on isotropic, which serves to reduce the overall strength of the final mixed fabric without having a strong influence on the pattern of SWS.

The formation of an HPG ice fabric is consistent with a stress regime of lateral compression across-flow and longitudinal extension along the ice flow direction. As ice undergoes viscous deformation the c-axes of the crystals rotate towards the axis of greatest compressive strain and away from the axis of extension [*Alley*, 1992]. *Minchew et al.* [2016] use satellite interferometry to extract the detailed surface strain-rate of Rutford Ice Stream. Their observations show that in our area of study there are along-flow positive deviatoric normal strain rates (extension) combined with significant across-flow negative deviatoric normal strain rates (compression). Ice flow with no lateral compression and pure longitudinal extension would form a thick girdle perpendicular to the ice flow direction. The addition of significant lateral compression causes c-axes to rotate towards the axis of compression, in the horizontal plane and across the flow, promoting the formation of HPG fabric. The stronger the lateral compression is in relation to the along-flow extension, the smaller the opening angle of the HPG (θ, Fig. 4a). The origin of the broad cluster fabric is less intuitive in this environment; it could be a remnant fabric from a previous stress regime that has not been completely modified; or a modification of the flow-induced HPG fabric by dynamic recrystallisation and polygonisation [*Gagliardini et al.*, 2009]. The splitting measurements are not frequency dependant (measurements are the same on data filtered to different bandwidths) and there is no clear 'double split' (when the shear waves are split twice by travelling though layers with different anisotropic properties) in these data. This suggests there are not two discrete layers, one of a cluster fabric and one of an HPG fabric and that the model can be well represented by a homogeneous anisotropic diffuse HPG medium.

As shown experimentally [*Pimienta et al.*, 1987], a macroscopic sample of ice with all the c-axes of its crystals orientated in the same direction deforms ten times faster than an equivalent isotropic sample, when it is sheared parallel to the basal planes. We determine the effect of the measured fabric on the mechanical properties of ice by considering it as a polycrystalline sample of ice containing 47% of the crystals in a pure HPG fabric and the rest isotropic (a reasonable approximation to a broad cluster), and assuming the uniform stress approximation of *Lliboutry* [1993]. Such a fabric results in ice which is 9.1 times easier to shear along the flow direction than horizontally across the flow direction.

Large-scale ice flow models (e.g. *Favier et al.* [2014]; *Deconto and Pollard* [2016]; *Gillet-Chaulet et al.* [2016]) assume that ice is isotropic. There are a number of justifications for this, other than our lack of knowledge about fabric or the numerical difficulty in incorporating anisotropy. A key justification is that the majority of *in situ* ice COF mea-

surements are made at ice domes or ridges. Ice COF in these areas is formed by horizontal shear and vertical compression, promoting the formation of cluster COF fabrics (Fig. 3a). Cluster fabrics are not rheologically anisotropic in the horizontal and therefore the overall effect of such an ice fabric can be simulated with a local change in viscosity, known as an enhancement factor [*Ma et al.*, 2010]. However, our observations of fabric in a fast flowing ice stream show a strong contrast in mechanical properties of the ice along and across the flow direction. The use of enhancement factors to assimilate ice viscosity changes is also justified when a flow regime does not change significantly over the time of a model simulation. Models tend to be initialised with known surface ice flow velocity data. Therefore, in a situation where ice flow conditions are stable over a model simulation, and thus the strain conditions are stable over this period, the final strain regime should be equivalent to the initialised one. However, we have evidence of recent changes in the direction of large Antarctic ice streams due to deglaciation (e.g., *Conway et al.* [2002]; *Bingham et al.* [2015]), leading to a possible misalignment between the flow-induced fabric and the present-day flow direction. In these cases the use of an enhancement factors is no longer a valid representation of ice viscosity. The mechanical properties of an ice fabric will also play an important role in ice fracture, for example during calving, which is an essential mechanism for rapid ice loss in Antarctica [*Pollard et al.*, 2015].

Ice streams, such as Rutford Ice Stream, which are characterised by initial convergent ice flow followed by lateral confinement along much of their length [*Minchew et al.*, 2016], are seen across much of Antarctica [*Ng*, 2015] and Greenland [*Bons et al.*, 2016]. It is therefore likely that the diffuse HPG fabric found here will be present in other fast-flowing ice stream environments. Ice streams are the key pathways of ice discharge from Antarctica and Greenland and therefore understanding how strain-induced ice fabric modifies the flow of ice in these regions in essential.

6 Conclusions

This is the first conclusive study of which we are aware that provides a robust model of ice stream fabric using shear wave splitting in microseismic data. A study on the downstream ice plain of Whillans Ice Stream [*Picotti et al.*, 2015] found that a weakly anisotropic cluster fabric dominated the entire ice depth and suggested that this may be typical of "large ice streams in regions where basal sliding and bed deformation dominate over internal glacial deformation". Here we provide clear evidence that this is not the case in Rutford Ice Stream, West Antarctica, which is also a large Antarctic ice stream moving primarily by basal sliding and sediment deformation [*Smith and Murray*, 2009]. Many of the commonly investigated ice fabrics in the literature thus far have been based upon those seen in ice cores, drilled at the interior of ice sheets. We have observed an additional category of ice fabric, the horizontal partial girdle, formed by strong horizontal confinement with longitudinal extension. In this study, we have provided new evidence of ice fabric structure in ice stream environments and shown that microseismic monitoring is an effective tool for investigating this. Neglecting such an ice fabric could lead to errors in modeled projections of ice flow, and thus reduce our ability to estimate the future contribution of ice sheets to sea level.

References

Alley, R. (1992), Flow-law hypotheses for ice-sheet modeling, *J. Glaciol.*, *38*, 245–256.

Alley, R. B. (1988), Fabrics in polar ice sheets: development and prediction, *Science*, *240*, 493–495, doi:10.1126/science.240.4851.493.

Azuma, N. (1994), A flow law for anisotropic ice and its application to ice sheets, *Earth Planet. Sci. Lett.*, *128*, 601–614, doi:10.1016/0012-821X(94)90173-2.

Bingham, R. G., D. M. Rippin, N. B. Karlsson, H. F. J. Corr, F. Ferraccioli, T. a. Jordan, A. M. Le Brocq, K. C. Rose, N. Ross, and M. J. Siegert (2015), Ice-flow structure and ice dynamic changes in the Weddell Sea sector of West Antarctica from radar-imaged internal layering, *J. Geophys. Res. Earth Surf.*, *120*, 655–670, doi:10.1002/2014JF003291.

Bons, P. D., D. Jansen, F. Mundel, C. C. Bauer, T. Binder, O. Eisen, M. W. Jessell, M.-G. Llorens, F. Steinbach, D. Steinhage, and I. Weikusat (2016), Converging flow and anisotropy cause large-scale folding in Greenland's ice sheet., *Nat. Commun.*, *7*, 11,427, doi:10.1038/ncomms11427.

Conway, H., G. Catania, C. Raymond, A. Gades, T. A. Scambos, and H. Engelhardt (2002), Switch of flow direction in an Antarctic ice stream, *Nature*, *419*, 456–467, doi:10.1038/nature01081.

Deconto, R. M., and D. Pollard (2016), Contribution of Antarctica to past and future sea-level rise, *Nature*, *531*(7596), 591–597, doi:10.1038/nature17145.

Diez, A., and O. Eisen (2015), Seismic wave propagation in anisotropic ice - Part 1: Elasticity tensor and derived quantities from ice-core properties, *The Cryosphere*, *9*, 367–384, doi:10.5194/tc-9-367-2015.

Duval, P., M. F. Ashby, and I. Andermant (1983), Rate-Controllng Processes in the Creep of Polycrystalline Ice, *J. Phys. Chem.*, *87*, 4066–4074, doi:10.1021/j100244a014.

Faria, S. H., I. Weikusat, and N. Azuma (2014a), The microstructure of polar ice. Part II: State of the art, *J. Struct. Geol.*, *61*, 21–49, doi:10.1016/j.jsg.2013.11.003.

Faria, S. H., I. Weikusat, and N. Azuma (2014b), The microstructure of polar ice. Part I: Highlights from ice core research, *J. Struct. Geol.*, *61*, 2–20, doi:10.1016/j.jsg.2013.09.010.

Favier, L., G. Durand, S. L. Cornford, G. H. Gudmundsson, O. Gagliardini, F. Gillet-Chaulet, T. Zwinger, A. J. Payne, and a. M. Le Brocq (2014), Retreat of Pine Island Glacier controlled by marine ice-sheet instability, *Nat. Clim. Change*, *5*(2), 117–121, doi:10.1038/nclimate2094.

Gagliardini, O., F. Gillet-Chaulet, and M. Montagnat (2009), A review of anisotropic polar ice models : from crystal to ice-sheet flow models, in *Physics of Ice Core Records, Vol. 2*, edited by T. Hondoh, Yoshioka, Kyoto, Japan.

Gillet-Chaulet, F., G. Durand, O. Gagliardini, C. Mosbeux, J. Mouginot, F. Rémy, and C. Ritz (2016), Assimilation of surface velocities between 1996 and 2010 to constrain the form of the basal friction law under Pine Island Glacier, *Geophys. Res. Lett.*, (1), 311–321, doi:10.1002/2016GL069937.

Harland, S. R., J. M. Kendall, G. W. Stuart, G. E. Lloyd, A. F. Baird, A. M. Smith, H. D. Pritchard, and A. M. Brisbourne (2013), Deformation in Rutford Ice Stream, West Antarctica: measuring shear-wave anisotropy from icequakes, *Ann. Glaciol.*, *54*, 105–114, doi:10.3189/2013AoG64A033.

Hill, R. (1952), The Elastic Behaviour of a Crystalline Aggregate, *Proc. Phys. Soc.*, *65*(5), 349–354, doi:10.1088/0370-1298/65/5/307.

Lliboutry, L. (1993), Anisotropic, transversely isotropic nonlinear viscosity of rock ice and rheological parameters inferred from homogenization, *Int. J. Plasticity*, *9*, 619–632.

Ma, Y., O. Gagliardini, C. Ritz, F. Gillet-Chaulet, G. Durand, and M. Montagnat (2010), Enhancement factors for grounded ice and ice shelves inferred from an anisotropic ice flow model, *J. Glaciol.*, *56*, 805–812, doi:10.3189/002214310794457209.

Matsuoka, K., D. Power, S. Fujita, and C. F. Raymond (2012), Rapid development of anisotropic ice-crystal-alignment fabrics inferred from englacial radar polarimetry, central West Antarctica, *J. Geophys. Res.*, *117*, 1–16, doi:10.1029/2012JF002440.

Maurel, A., F. Lund, and M. Montagnat (2015), Propagation of elastic waves through textured polycrystals: application to ice, *Proc. R. Soc.*, *471*, 1–28, doi:10.1098/rspa.2014.0988.

Minchew, B. M., M. Simons, B. Riel, and P. Milillo (2016), Tidally induced variations in vertical and horizontal motion on Rutford Ice Stream, West Antarctica , inferred from remotely sensed observations., *J. Geophys. Res. Earth Surf.*, *122*, 167–190, doi:10.1002/2016JF003971.

Murray, T., A. M. Smith, M. A. King, and G. P. Weedon (2007), Ice flow modulated by tides at up to annual periods at Rutford Ice Stream, West Antarctica, *Geophys. Res. Lett.*, *34*, 1–6, doi:10.1029/2007GL031207.

Nanthikesan, S., and S. Shyam Sunder (1994), Anisotropic elasticity of polycrystalline ice Ih, *Cold Reg. Sci. and Tech.*, *22*(2), 149–169, doi:10.1016/0165-232X(94)90026-4.

Ng, F. S. L. (2015), Spatial complexity of ice flow across the Antarctic Ice Sheet, *Nat. Geosci.*, *8*, 847–852, doi:10.1038/NGEO2532.

Picotti, S., A. Vuan, J. M. Carcione, H. J. Horgan, and S. Anandakrishnan (2015), Anisotropy and crystalline fabric of Whillans Ice Stream (West Antarctica) inferred from multicomponent seismic data, *J. Geophys. Res. Solid Earth*, *120*(6), 4237–4262, doi:10.1002/2014JB011591.

Pimienta, P., P. Duval, and V. Y. Lipenkov (1987), Mechanical behavior of anisotropic polar ice, in *The Physical Basis of Ice Sheet Modelling (Proceedings of the Vancouver Symposium)*, pp. 57–66.

Pollard, D., R. M. DeConto, and R. B. Alley (2015), Potential Antarctic Ice Sheet retreat driven by hydrofracturing and ice cliff failure, *Earth and Planet. Sci. Lett.*, *412*, 112–121, doi:10.1016/j.epsl.2014.12.035.

Savage, M. K. (1999), Seismic anisotropy and mantle deformation: What have we learned from shear wave splitting?, *Rev. Geophys.*, *37*(1), 65–106, doi:10.1029/98RG02075.

Silver, P. G., and W. W. Chan (1991), Shear wave splitting and subcontinental mantle deformation, *J. Geophys. Res.*, *96*, 16,429–16,454, doi:10.1029/91JB00899.

Smith, A. (1997), Basal conditions on Rutford Ice Stream, West Antarctica, from seismic observations, *J. Geophys. Res.*, *102*(B1), 543–552, doi:10.1029/96JB02933.

Smith, A. M. (2006), Microearthquakes and subglacial conditions, *Geophys. Res. Lett.*, *33*, 1–5, doi:10.1029/2006GL028207.

Smith, A. M., and T. Murray (2009), Bedform topography and basal conditions beneath a fast-flowing West Antarctic ice stream, *Quat. Sci. Rev.*, *28*, 584–596, doi:10.1016/j.quascirev.2008.05.010.

Smith, E. C., A. M. Smith, R. S. White, A. M. Brisbourne, and H. D. Pritchard (2015), Mapping the ice-bed interface characteristics of Rutford Ice Stream , West Antarctica, using microseismicity, *J. Geophys. Res. Earth Surf.*, *120*, 1881–1894, doi:doi:10.1002/2015JF003587.

Teanby, N. A., J. M. Kendall, and M. Van der Baan (2004), Automation of shear-wave splitting measurements using cluster analysis, *Bull. Seismol. Soc. Am.*, *94*, 453–463, doi:10.1785/0120030123.

Wuestefeld, A., O. H. Al-Harrasi, J. P. Verdon, J. Wookey, and J.-M. Kendall (2010), A strategy for automated analysis of passive microseismic data to image seismic anisotropy and fracture characteristics, *Geophys. Prosp.*, *58*, 755–773, doi:10.1111/j.1365-2478.2010.00891.x.

Figure 1.   Earthquake locations on Rutford Ice Stream showing the location of seismic events and typical event waveform. a) Map is in south pole stereographic projection. Purple dots show the location of ~3000 microseismic events generated at the base of the ice stream over a 32-day period. Many events occur in close proximity and overlap in this figure. Location of three-component geophones are red triangles, the orientation of the two horizontal components (X and Y) are shown. Background is Landsat Image Mosaic of Antarctica (LIMA). White arrow shows ice flow direction. b) The waveform of a typical basal microseismic seismic event recorded at a geophone with labelled components. Strong shear waves can be seen on the horizontal components and a clear shear wave split can be seen with shear wave 'S1' arriving on the cross-stream component (X) before shear wave 'S2' arriving later on the down-stream component (Y).

135 **Figure 2. Upper hemisphere plot of splitting measurements.** Splitting measurements (bars) are plotted at
136 their event to station azimuth from north (clockwise around the plot) and ray-path inclination, with the centre
137 of the plot being vertical (0°) and the edge of the plot being horizontal (90°). Measurements are smoothed
138 by taking the average of the measurements in inclination and azimuth bins of 5°× 5°. The orientation of each
139 bar represents the polarisation direction of the fast shear wave (Φ) for a given measurement. The length and
140 colour of each bar represents δV_s, percentage S-wave velocity deviation from the isotropic S-wave velocity.
141 The maximum inclination at which good quality measurements were observed was 73°, hence there are no
142 measurements at the outermost edges of the plot.

181   **Figure 3. SWS parameters expected for different ice fabrics**. Left Hand Side: Schematic for each fabric
182   type (adapted from *Maurel et al.* [2015] and *Diez and Eisen* [2015]), with the envelope of c-axes (blue area)
183   and the projection of these c-axes on an upper hemisphere plot (blue dots on the horizontal plane). The angles
184   ξ and θ are used to describe the opening angle of the c-axes envelopes in the X_1 and X_2 directions respec-
185   tively. Right Hand Side: δV_s - the strength of anisotropy (background colour) and direction of the fast shear
186   wave for each fabric type (black bars) on an upper hemisphere plot a) Cluster with an opening angle $\theta = 30°$.
187   b) Thick girdle with opening angle of $\xi = 15°$ c) Vertical partial girdle with an opening angle of $\theta = 15°$. d)
188   Horizontal partial girdle with an opening angle of $\theta = 15°$.

Figure 4. **Ice fabric model from shear wave splitting measurements** a) Horizontal partial girdle fabric which makes up 47% of the best fit fabric mixture. Left Hand Side: A schematic of the ice fabric, the envelope of c-axes is within the blue volume, the projection of these c-axes on an upper hemisphere plot is shown (blue dots on the horizontal plane). Right Hand Side: An upper hemisphere plot of modeled shear wave propagation through this fabric, black bars represent the orientation of the fast shear wave and the background colour represents δV_s. Maximum δV_s for this fabric is 9.3%. The orientation of the girdle is near perpendicular to the ice flow direction. b) Broad cluster fabric which makes up 53% of the best fit fabric mixture - the diagram is as in (a). This fabric is weakly anisotropic with a maximum δV_s of 2.1%. c) Best fitting ice fabric model the 'diffuse HPG' - a mixture of 47% horizontal partial girdle and 53% broad cluster. Coloured background and black bars show modeled data. Measured shear wave splitting measurements (coloured bars) are overlain to show fit. Note that the colour scales are different in a, b and c to maximise resolution.

Figure 1.

a

b
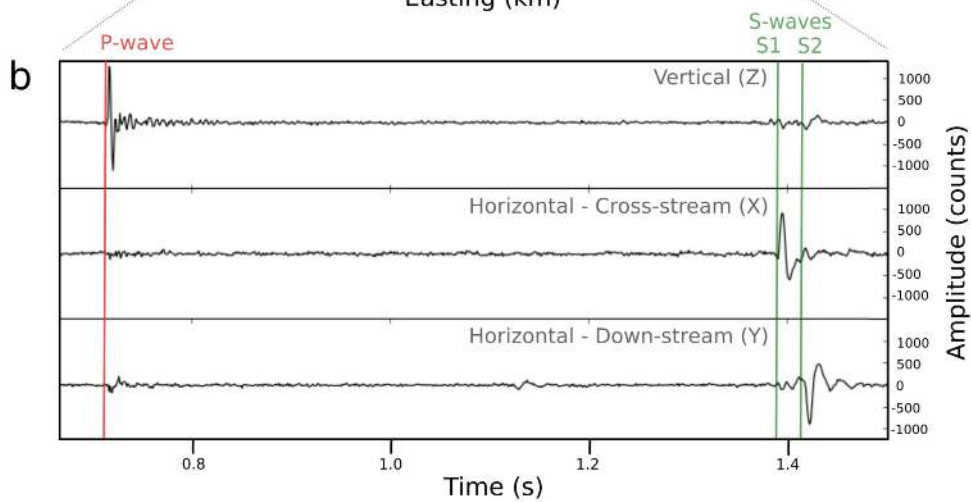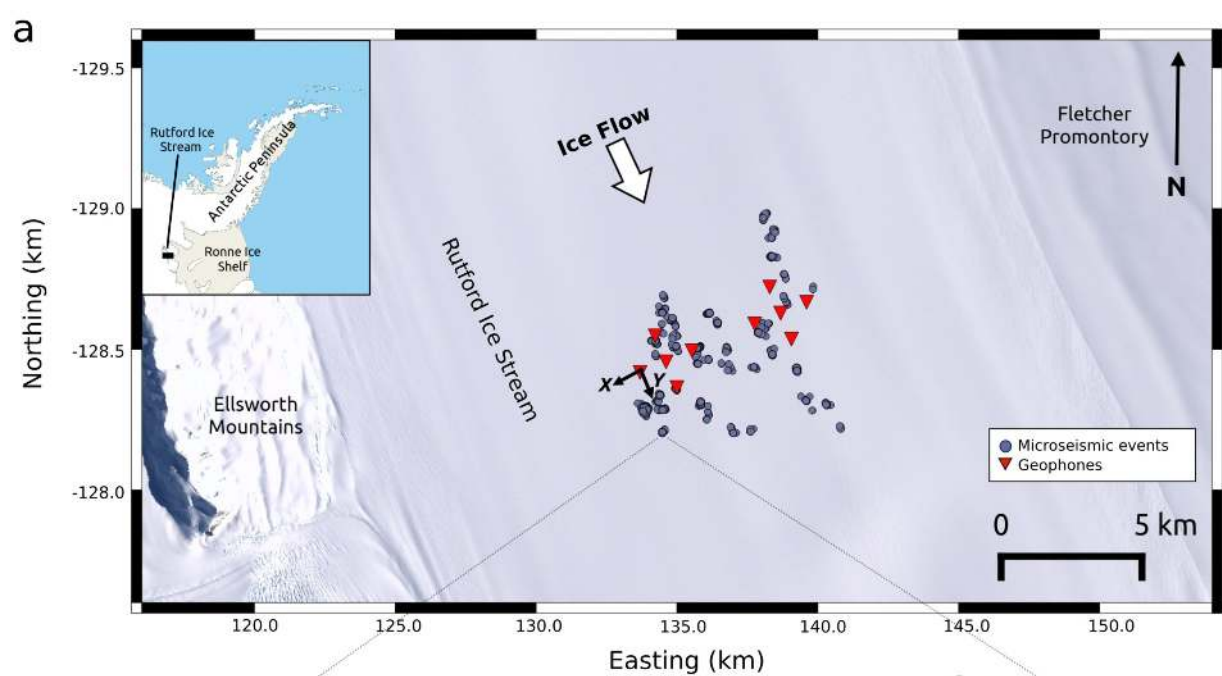
Figure 2.

Figure 3.

a) Cluster

$\theta = \xi$
$0 < \theta < 90$

b) Thick Girdle

$\theta = 90$
$0 < \xi < 90$
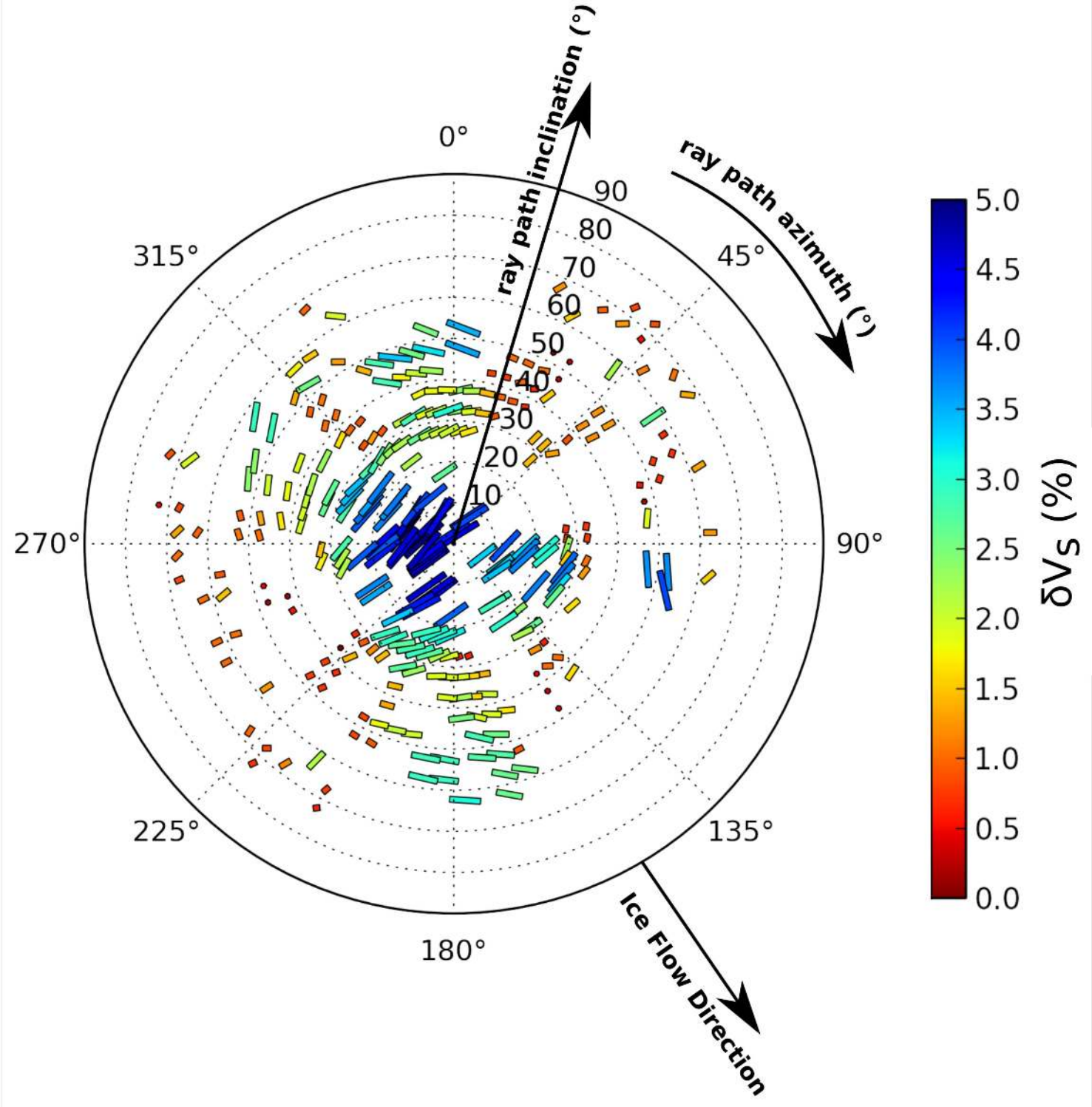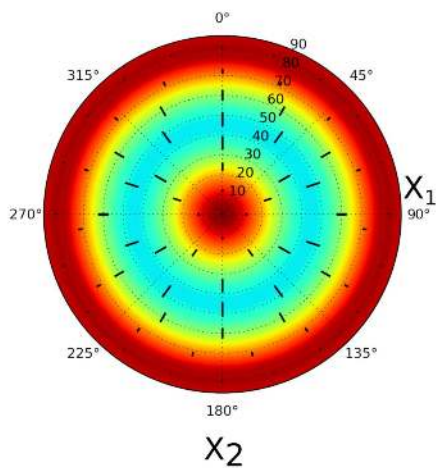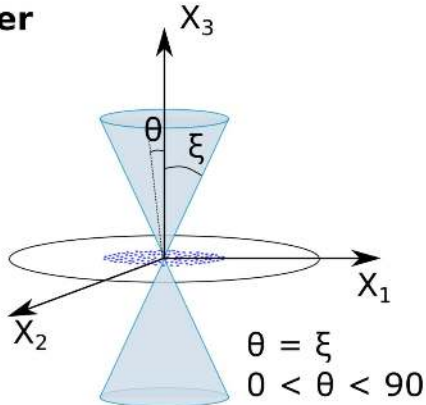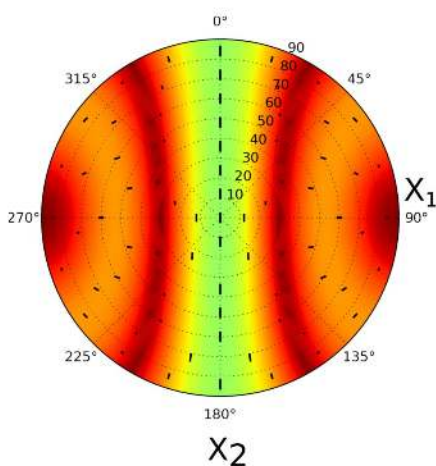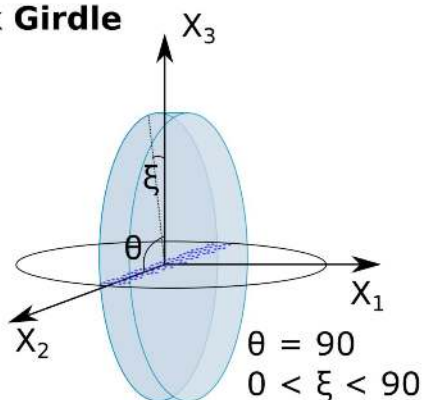
c) Vert. Partial Girdle

$\xi = 0$
$0 < \theta < 90$
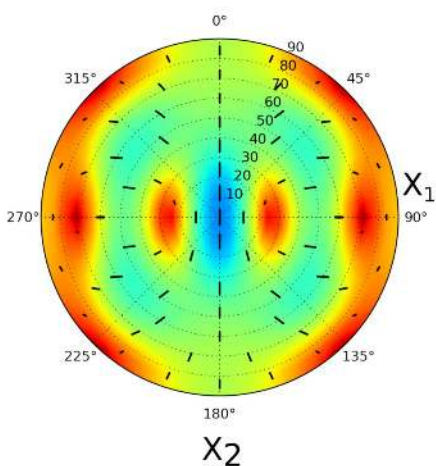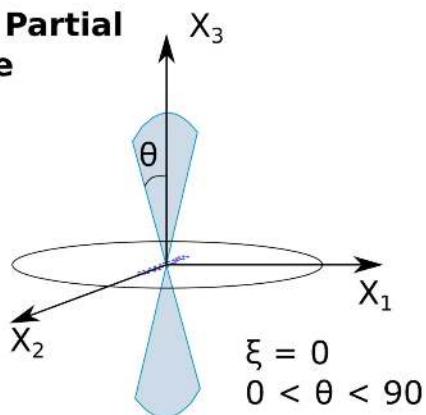
d) Horiz. Partial Girdle

$\xi = 0$
$0 < \theta < 90$

δV_S (%)
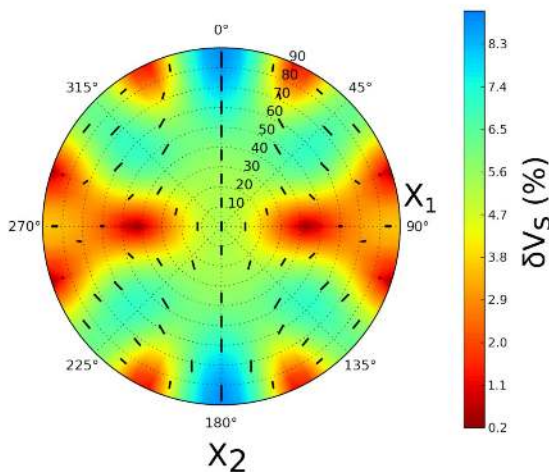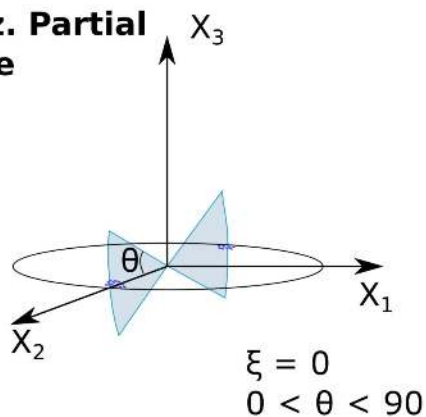
Figure 4.

a) Modeled horizonal partial girdle fabric (HPG)

$\theta = 22°, \xi = 0°$
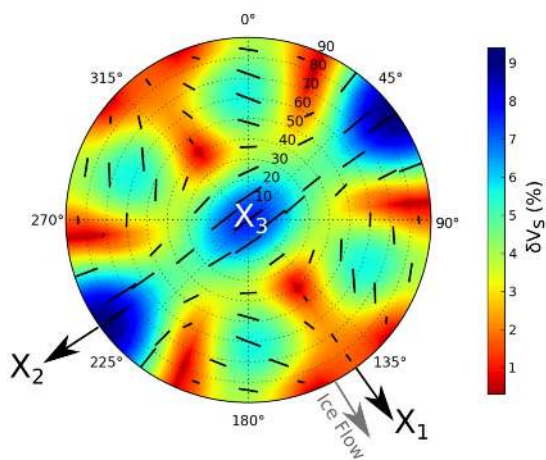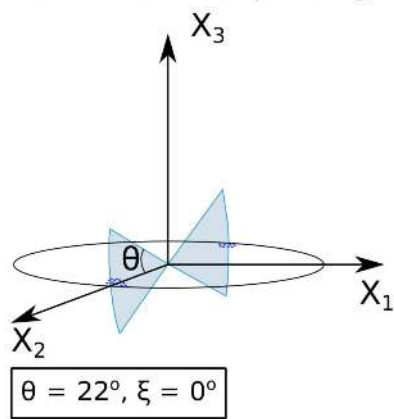
b) Modeled cluster fabric

$\theta = \xi = 73°$
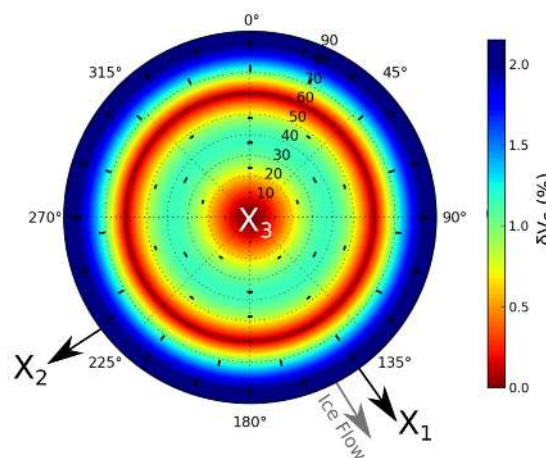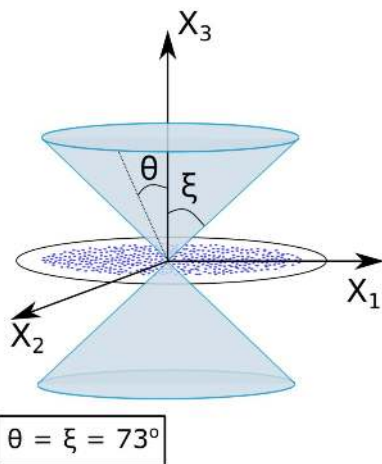
c) Modeled "Diffuse HPG" fabric (background) with SWS measurements (overlay)
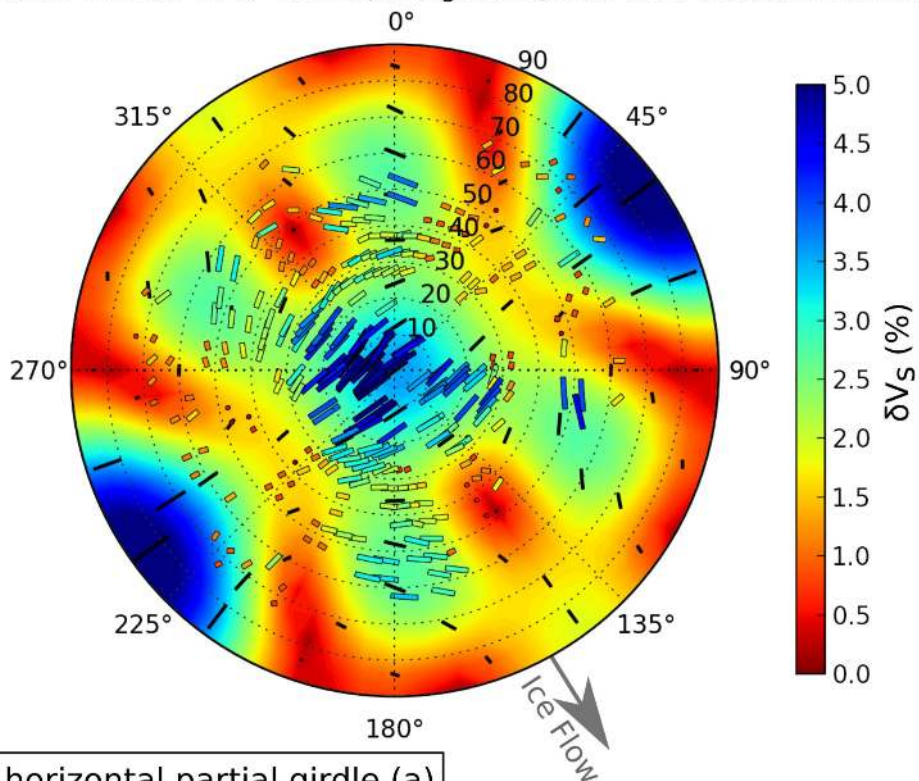
47% horizontal partial girdle (a)
53% cluster (b)